Capillary porosity depercolation in cement-based materials: Measurement techniques and factors which influence their interpretation

Gaurav Sant [a,*], Dale Bentz [b,1], Jason Weiss [c,2]

[a] Department of Civil and Environmental Engineering, University of California, Los Angeles, Los Angeles, CA, USA
[b] Engineering Laboratory, Materials and Construction Research Division, National Institute of Standards and Technology, 100 Bureau Drive, Stop 7313, Gaithersburg, MD, USA
[c] Pankow Materials Laboratory, Purdue University, School of Civil Engineering, 550 Stadium Mall Drive, West Lafayette, IN, USA

ARTICLE INFO

ABSTRACT

The connectivity of the capillary porosity in cement-based materials impacts fluid-and-ion transport and thus material durability, the interpretation of experimental measurements such as chemical shrinkage, and the timing and duration of curing operations. While several methods have been used to assess the connectivity of the capillary pores, the interpretation of some experimental procedures can be complicated by the addition of certain chemical admixtures. This paper assesses capillary porosity depercolation in cement pastes using measurements of chemical shrinkage, low temperature calorimetry (LTC), and electrical impedance spectroscopy. The experimental results are analyzed to identify the time of capillary porosity depercolation. In addition, the factors that influence the interpretation of each technique are discussed. Experimental evidence suggests that capillary porosity depercolation, as defined by Powers, occurs after hydration has reduced the capillary porosity to around 20% in cement paste systems. The influence of capillary porosity depercolation on the transport properties is demonstrated in terms of a reduction in the electrical conductivity of the cementitious material. Special attention is paid to understand and interpret the influence of shrinkage-reducing admixtures (SRAs) on the freezing behavior of cementitious systems, particularly in regard to the inapplicability of using LTC to detect porosity depercolation in cement pastes containing such organic admixtures.

1. Introduction and background

The desire to increase the service-life of civil engineering infrastructure has led in many cases to the increased use of low *w/c* (water-to-cement ratio) concretes in construction. However, low *w/c* concretes are not without problems, as the refined pore size distribution of these materials amplifies autogenous shrinkage, magnifying the risk of cracking at early-ages [1,2]. To minimize the risk of early-age cracking several approaches have been developed including: (1) internal curing using water reservoirs such as pre-wetted lightweight aggregates or superabsorbent polymers [3–5], (2) the extension of recommended wet curing durations during construction [6,7], (3) the use of shrinkage-reducing admixtures (SRAs) to reduce capillary stress development [8–10] and (4) the

utilization of expansive cements or additives that can generate an expansion to mitigate tensile stress development at early ages [11,12].

Curing is carried out to provide sufficient water for binder hydration and limit the impact of self-desiccation in cementitious materials. However, this assumes that water is able to freely migrate through the concrete to locations where it may be needed to promote hydration and maintain saturation [13,14]. While this assumption may be reasonable for concretes with a higher *w/c* (e.g., 0.45 and greater), it may not be the case for low *w/c* mixtures, when the capillary pore-structure may become discontinuous [15–17]. For example: in the case of internal curing, if moisture is released from curing reservoirs after the capillary pore-structure has disconnected, the distance that water can travel may be considerably limited [13,14]. For external curing, if the capillary porosity disconnects prior to or during curing, moisture would be unable to penetrate the full depth of the concrete, limiting curing effectiveness to the topmost portions of the covercrete.

These concerns demonstrate the need for a more complete understanding of capillary porosity depercolation/disconnection in cement-based materials. Since it is recognized that the porosity within cement-based materials always remains percolated when the gel pores are considered, here, consistent with the original work of Powers *et al.* [15,18], it is depercolation or discontinuity of the

* Corresponding author. Tel.: +1 310 206 3084; fax: +1 301 206 2222.
 E-mail addresses: gsant@ucla.edu (G. Sant), dale.bentz@nist.gov (D. Bentz), wjweiss@purdue.edu (J. Weiss).
[1] Tel.: +1 301 975 5865; fax: +1 301 990 6891.
[2] Tel.: +1 765 494 2215; fax: +1 765 494 0395.

capillary pores or original water-filled spaces between cement particles that is considered.[3] Importantly, in addition to water curing, depercolation effects also have implications on the transport properties and durability response of structures. While porosity depercolation was first assessed on the basis of fluid-permeability measurements [15], it has also been assessed experimentally using measurements of chemical shrinkage and low temperature calorimetry (LTC), or numerically using computer simulation models [16,17,19,20].

This study assesses capillary porosity depercolation in cement pastes using measurements of chemical shrinkage, electrical conductivity and low temperature calorimetry for low w/c pastes which are expected to depercolate (w/c = 0.30) and a high w/c paste that retains a percolated microstructure (w/c = 0.50) as based on Powers analysis. Special attention is paid to understand the influence of SRAs on LTC measurements and on interpreting capillary porosity depercolation using this technique. This investigation has significant implications for the development of curing strategies for low w/c concretes and for simulating moisture ingress and ion-transport in cementitious materials.

2. Materials and mixing procedures

Three different cement paste mixtures were prepared using the mixture proportions shown in Table 1. An ASTM C150 type I ordinary portland cement (OPC) was used with a Blaine fineness of 360 m^2/kg and an estimated Bogue phase composition (mass fraction) of 60% C_3S, 12% C_2S, 12% C_3A, and 7% C_4AF, with a Na_2O equivalent of 0.72%.

To enhance the workability of the cement paste mixtures, a high range water reducing admixture (HRWRA, Glenium 3000NS) was used. A commercial shrinkage-reducing admixture (SRA, Tetraguard AS20) was added at a 5% concentration of the initial water-SRA solution (by mass replacement). The particle size distribution of the cement as measured by laser diffraction using isopropanol as a powder dispersant is shown in Fig. 1. For measurements of chemical shrinkage and electrical conductivity, de-aired, neat cement pastes were prepared using de-ionized water [21]. For measurements of LTC, cement pastes were prepared using the Portland Cement Association (PCA) procedure, as adopted by NIST. The mixing procedures are presented in greater detail elsewhere [22,23].

3. Experimental procedures

Several experimental procedures were used to characterize the pore-structure and connectivity of water-filled capillary pores in cement pastes at early ages. Specifically, chemical shrinkage studies were used to identify the influence of hydration on water absorption, while electrical conductivity and LTC datasets were used to assess the transport properties and the connectivity and volume of accessible moisture available in the material respectively. Unless noted otherwise, all the experiments were performed at room temperature, i.e., between 20 °C to 23 °C.

3.1. Chemical shrinkage of cement pastes

Chemical shrinkage was measured according to the buoyancy principle for paste specimens of varying thicknesses (3 mm, 12 mm, and 24 mm) to ascertain the influence of specimen thickness on the measured chemical shrinkage response [21]. The fresh cement paste was placed in a glass crystallization dish, which was then suspended from a balance plate immersed in paraffin oil contained in a temperature-controlled bath. Each specimen was ponded with 10 g

Table 1
Mixture proportions (mass fraction).

Mixture ID	w/c = 0.30	w/c = 0.30SRA	w/c = 0.50
OPC (ASTM C150 Type I)	1.0000	1.0000	1.0000
DI-Water	0.3000	0.2850	0.5000
HRWRA (Glenium 3000NS[**])	0.0053	0.0053	–
SRA (Tetraguard AS20)	–	0.0150	–

[**] Commercial Equipment, instruments, and materials mentioned in this manuscript are identified only for the sake of clarity and to foster understanding. Such identification does not imply recommendation or endorsement by the University of California, Los Angeles, Purdue University, or the National Institute of Standards and Technology nor does it imply that the specific materials or equipment identified are the best available for the purpose.

of surface water prior to immersion in the paraffin bath. The measured change in mass was then used to assess the extent of chemical shrinkage experienced by the cement paste. The measured chemical shrinkage was used to determine the rate and degree of hydration of the cement paste, assuming 0.064 ml of chemical shrinkage per gram of cement completely reacted [24]. The coefficient of variation of the measurements is estimated to be 5%, based on the chemical shrinkage of duplicate specimens measured at 48 h. It should be noted that the chemical shrinkage specimens were permitted to absorb water over the time the test was performed [21]. Due to the varying specimen thicknesses evaluated, the thin specimens cured under saturated conditions, while the thick specimens experienced a combination of saturated and partially saturated curing conditions due to the inability of water to penetrate to the bottom of the sample due to the depercolation of the capillary porosity, as will be presented subsequently. However, this difference in curing conditions had a small influence on the extent of reaction experienced up to 24 h, as the degree of hydration calculated from chemical shrinkage showed good agreement with measurements of isothermal calorimetry performed under sealed conditions.

3.2. Electrical conductivity of cement pastes and extracted pore solutions

The electrical conductivity of the cement pastes was measured using cylindrical paste specimens (22 mm diameter, 50 mm height) to determine the time-dependent change in the connectivity of the microstructure. The specimens were cast and stored in airtight vials. Two stainless steel electrodes (2.5 mm diameter rods spaced 10 mm center to center) were embedded longitudinally inside each vial. A Solartron 1260™ Impedance Gain-Phase analyzer measured the electrical impedance response of each specimen. The measurements were made over the frequency range of 10 MHz to 1 Hz (10 steps/ frequency decade) using a 100 mV AC stimulus. The bulk resistance (R_b, ohms) obtained from the frequency-dependent electrical
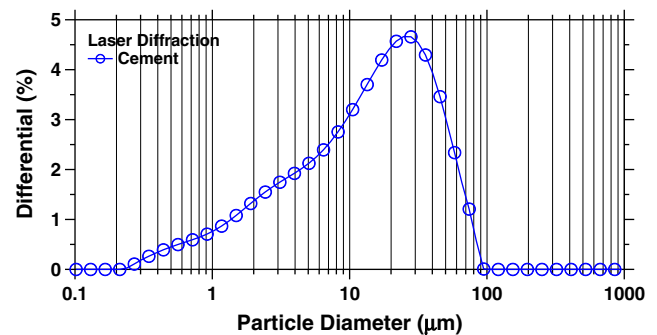
Fig. 1. The particle size distribution of the cement used in this investigation as measured using laser diffraction. The results shown are the average of six individual measurements and the error bars (one standard deviation) would fall well within the size of the shown symbols.

---

[3] Here too, consistent with the original definition of Powers and co-workers, gel pores are assumed to have a pore diameter of around 2 nm while the capillary pores encompass a pore diameter range between 10 and 1000 nm [18].

impedance response was used to determine the material's bulk electrical conductivity after normalizing for the effects of specimen and electrode geometry using Eq. (1):

$$\sigma_t = \frac{k}{R_b} \tag{1}$$

where: σ_t is the bulk paste conductivity (S/m) and k is a cell geometry factor ($15.76 \pm 0.01 \, \text{m}^{-1}$) that was determined experimentally [25,26]. Data acquisition was performed automatically at 20 min intervals from a half an hour after mixing up to an age of 48 h. During the measurements, the specimens remained sealed inside plastic vials to minimize moisture loss and its influence on the measured conductivity. Each vial was partially immersed in a water bath to maintain the specimen's temperature at 23 °C ± 1 °C. The coefficient of variation of the measurements is estimated to be 6%, based on the conductivity of duplicate specimens measured at 48 h.

Pore solution was extracted from cement pastes ($w/c = 0.30$, $w/c = 0.30$SRA) using nitrogen pressure filtration or a high pressure steel die. Pressure filtration was performed for specimens in the plastic phase (until 6 h after water addition) according to the procedure of [27]. For hardened specimens, a steel extraction die with a capacity of 550 MPa was used according to the procedure described in [28]. After extraction, the pore solution was sealed in small (25,000 mm³) plastic containers to minimize the potential for carbonation. The pore solution conductivity (σ_o) was measured using a conductivity cell connected to the impedance analyzer. The pore solution conductivity of the $w/c = 0.50$ cement paste was obtained from data previously published in the literature for a cement having a similar Bogue potential phase composition [29].

3.3. Low temperature calorimetry of cement pastes, porous glasses and bulk solutions

The first series of experiments consisted of LTC performed on cement pastes to determine the volume and connectivity of the available freezable water [19]. Approximately 10 g of cement paste was sealed in an air-tight vial and provided with a layer of surface water to provide 'saturated' curing conditions. At the desired specimen age, the paste was crushed and a small surface-dried specimen (≈ 100 mg) was extracted. The specimen was then placed in a stainless steel pan, and with another reference pan was placed in the calorimeter cell. The sample was first equilibrated to -10 °C and then equilibrated to $+5$ °C [34]. A freezing scan was conducted from $+5$ °C to -55 °C at a cooling rate of 0.5 °C/min. As per the specifications of the manufacturer, the differential scanning calorimeter used has a sensitivity of $\pm 2.5\%$ and a baseline noise of 1.5 μW.

The second series of experiments consisted of LTC performed on two porous glass specimens having a nominal monosize pore radius of 200 nm and 4 nm, respectively, to determine the influence of mono versus distributed pore sizes on the results. Experiments were performed on specimens saturated with DI-water, a synthetic pore solution (0.35 M KOH + 0.05 M NaOH), and DI-water and synthetic pore solution containing various concentrations (i.e., 5%, 10% and 20%) of SRA. In an attempt to minimize degradation of the porous glass by the pore solution, specimens were saturated over-night and the LTC performed the following day. For the porous glass, the sample was first equilibrated to -10 °C and then equilibrated to $+5$ °C. A freezing and melting scan was then conducted from $+5$ °C to -75 °C to $+5$ °C at a cooling or heating rate of 0.5 °C/min.

The third series of experiments consisted of LTC performed on solutions with and without SRA to determine the influence of the admixture on the freezing and melting response of bulk solutions. As such, three solutions: de-ionized water and two other solutions containing 10% and 20% SRA in water were placed in a stainless steel pan, which was sealed and with a reference pan then placed in the calorimeter cell. The sample was first equilibrated to -10 °C and then equilibrated to $+5$ °C. A freezing and melting scan was then conducted on the bulk solutions from $+5$ °C to -25 °C to $+5$ °C at a cooling or heating rate of 0.5 °C/min.

4. Experimental results

4.1. Chemical shrinkage of cement pastes

Fig. 2 shows the measured chemical shrinkage as a function of specimen age for specimens of varying thickness for a plain cement paste and a paste containing SRA; both having a $w/c = 0.30$. In general, a decreasing magnitude of chemical shrinkage is observed, at later ages, with increasing specimen thickness. This occurs due to pore refinement, whereby the fluid-saturated thickness of the specimen changes (reduces) with time [21]. A similar effect was noted by Geiker and was observed to be magnified in mixtures containing fine cements or little water (low w/c) [20,30]. However, measurements of non-evaporable water content performed to determine the impact of water availability on cement hydration showed smaller discrepancies through the depth of the specimen [21]. The change in the post-deviation slope of the chemical shrinkage curves which decreases
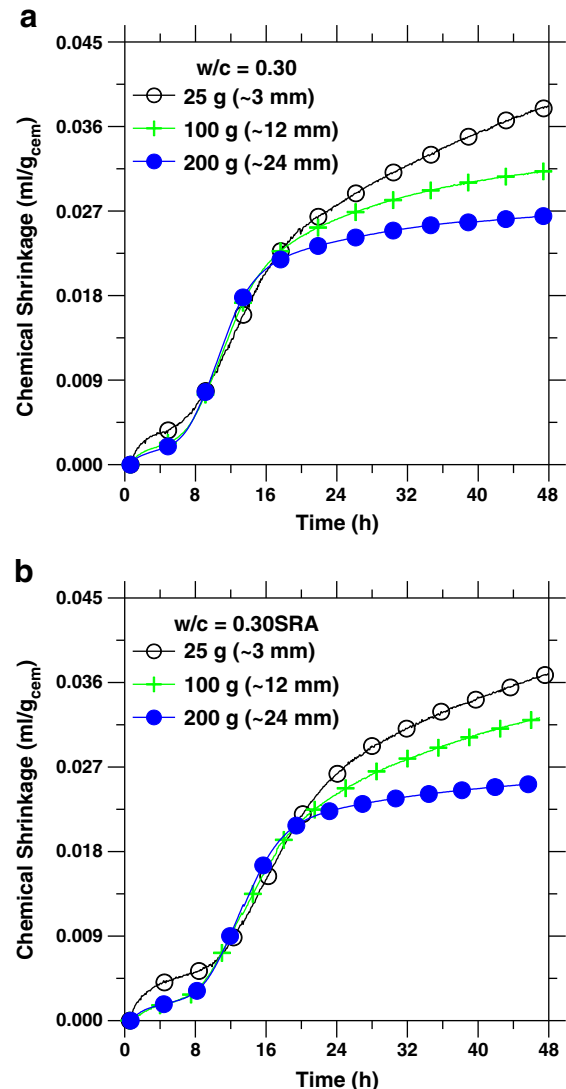

Fig. 2. Chemical shrinkage as a function of specimen age for cement paste mixtures for specimens of varying thicknesses: (a) $w/c = 0.30$ and (b) $w/c = 0.30$SRA.

with increasing specimen thickness indicates a change in the rate of water penetration and a smaller effect which is related to differences in the average rate of cement hydration in the thin and thick specimens after the capillary pore structure has depercolated. Here, depercolation is being inferred as corresponding to the point at which the water imbibition rate of the thicker paste specimens can no longer keep up (and thus deviates) with the ongoing cement hydration requirements of that particular paste mixture.[4] Similar divergences have been observed when comparing the chemical shrinkage of thick specimens to isothermal calorimetry or non-evaporable water content measurements, with the divergence occurring at later ages for higher w/c pastes [31], consistent with the porosity discontinuity inferences of Powers [15].

Both low w/c mixtures show a dependence of chemical shrinkage on paste thickness, wherein the measured values of chemical shrinkage for the thicker specimens begin to plateau before those for the thin specimens. This size-dependent deviation occurs at approximately 18 h and 21 h for the plain paste (Fig. 2(a)) and the SRA paste (Fig. 2(b)), respectively, and indicates a change in the connectivity of the pore-structure with increasing hydration. The delay in the deviation experienced by the SRA paste compared to the plain paste is attributed to the slight delay in hydration and the change in the fluid-transport properties induced by the SRA [32,33]. The chemical shrinkage measured for a $w/c = 0.30$ paste (around 3 mm thick with no chemical admixtures) was used to infer the degree of hydration of the $w/c = 0.50$ paste while assuming that in the first 24 h, the chemical shrinkage and degree of hydration of pastes in the range $w/c = 0.30$–0.50 is similar [34–36]. Other chemical shrinkage datasets developed for cement pastes of varying w/c (between 0.30–0.60) also indicate that the longer-term (14 days) chemical shrinkage of SRA pastes is slightly higher than that of plain pastes at an equivalent w/c; for $w/c < 0.50$ [37].

4.2. Electrical conductivity of cement pastes and pore solutions

Fig. 3(a) shows the bulk paste conductivity for the three cement paste mixtures. It is seen that for each mixture, the conductivity first briefly increases due to the initial dissolution of the alkali sulfates into the mixing water. After this time, the bulk conductivity decreases. The reduction in the conductivity is noted to occur at a similar rate for the low w/c mixtures, but at a slower rate for the high w/c mixture. The conductivity at 48 h ranks as 0.30SRA:0.30:0.50 (see mixture details in Table 1) in order of increasing paste conductivity.

Fig. 3(b) shows the measured pore solution conductivity as a function of specimen age for the paste mixtures. For the three mixtures, four distinct stages in the conductivity response were observed. In the first stage, the pore solution conductivity increases rapidly due to the dissolution of the alkali sulfates into the mixing water. In the second stage, the conductivity remains almost constant. Chemical analysis of the pore solution confirms that the concentration of ions in solution remains approximately constant during this period [32,33]. During the third stage, a rapid increase in the solution conductivity occurs which corresponds to a significant increase in the solution's ion-concentration over this time-period. In the final (fourth) stage beyond 24 h, the conductivity of the pore solution continues to increase, but at a slower rate [25].

---

[4] It should be clarified that 'capillary depercolation' is not intended to indicate a unique point of time at which the connectivity of the porosity is abruptly reduced. Rather this is a gradual process which progresses incrementally as the cement hydrates and the porosity refines. Further, it should be clarified that this aspect is restricted to the capillary pores only as at the scale of the gel-pores the porosity is perpetually connected.
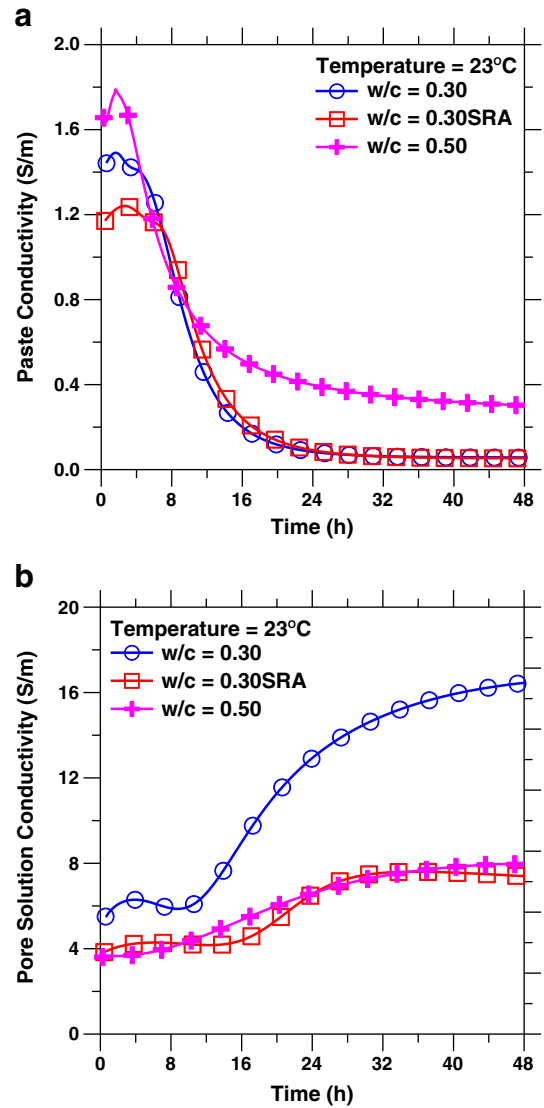

Fig. 3. The measured electrical conductivity measured as a function of specimen age for: (a) cement pastes and (b) extracted pore solutions.

4.4. Low temperature calorimetry

Fig. 4 shows heat flow as a function of temperature for LTC scans performed on plain cement paste ($w/c = 0.30$) samples at several ages. Prior to a specimen age of 14 h, only one peak is observed and it occurs
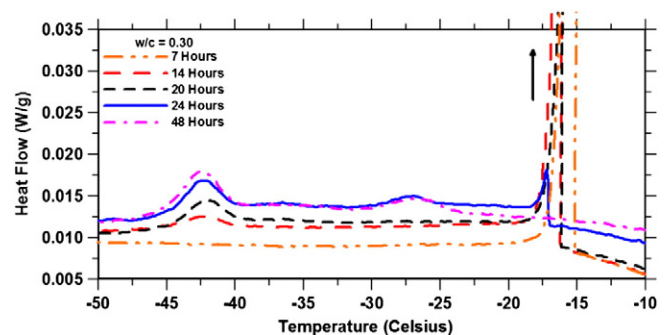

Fig. 4. Representative LTC Scans for a plain cement paste ($w/c = 0.30$) at several ages.

near -15 °C in the LTC scan. After the specimen achieves an age of 14 h, two peaks are observed with the first near −15 °C and the second −43 °C. The peak at −15 °C is still much larger than the peak at −43 °C. With increasing age, the peak at −43 °C is observed to increase in magnitude, while the peak at −15 °C decreases in magnitude. The decrease in the magnitude of the −15 °C peak with increasing age indicates a reduction in the volume and connectivity of freezable water contained in the percolated capillary pores [19,39]. At an age of 24 h, a new peak appears at −27 °C and the peaks at −15 °C and −43 °C are observed to have a similar magnitude. Finally, the −15 °C peak is observed to disappear between 24 h and 48 h. The peak at −27 °C would similarly disappear at later ages beyond 48 h, while the peak at −43 °C would achieve a maximum and then progressively decrease in size [18,34].

Fig. 4 illustrates datasets for cement paste exposed to a single freezing scan that are typical of those for neat cement pastes and concretes as reported previously [18,34,38]. Specific aspects of this peak behavior have been previously attributed to qualitative microstructural features of the cement paste. The peak that occurs around −15 °C indicates solution freezing, in a heterogeneous fashion, in the percolated (water-filled) capillary pores. The peak that occurs around −27 °C indicates solution freezing in the open gel pores and in capillary pores that are completely surrounded by such gel pores (corresponding to the classic ink-bottle response). The peak around −43 °C corresponds to solution freezing in pores that is induced by homogenous ice nucleation [39–41]. This peak could include contributions of ice formation in the capillary pores and larger gel pores that are surrounded by entryways smaller than the limiting curvature that can be achieved by an intruding ice-lens [40]. The specific temperatures at which these peaks are often observed have been noticed to vary slightly depending on the solution composition and freezing-rate effects in the pore-fluid.

It should be noted, in the present study, that the focus is only on identifying the presence-or-absence of the first peak at −15 °C, as no attempt is being made to estimate the pore size distributions as determined using thermoporometry [35,40,42,43]. As such, the presence or absence of the freezing peak at −15 °C is being related to the connectivity of pore solution contained in the capillary pores [18]. Qualitatively, this behavior can be compared to the chemical shrinkage measurements that show a deviation as a function of age and specimen thickness (Fig. 2).

An advantage of LTC in evaluating the pore-structure of cement-based materials is that it does not require aggressive drying, unlike mercury porosimetry for example [44]. However, LTC only detects pores that contain solution. Consequently, this technique is incapable of detecting vapor filled porosity that develops due to self-desiccation in sealed specimens or thicker specimens that experience partial saturation. In addit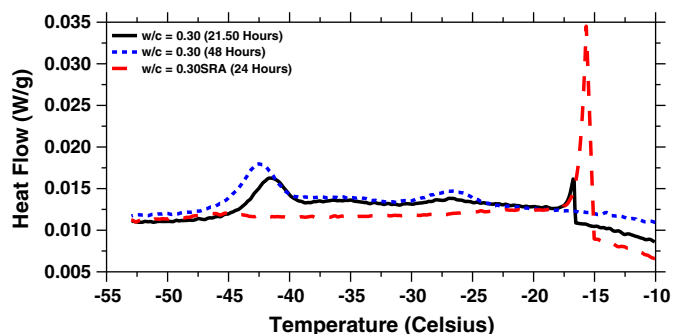ion to plain pastes ($w/c = 0.30$), LTC scans were performed on SRA containing pastes ($w/c = 0.30$SRA) to determine the change in freezable water content in this system. As seen in Fig. 5, the LTC scans are considerably different from those in the plain paste system when a SRA is present in the paste [45]. At 24 h, while the SRA system (equivalent age of 21.5 h for the plain paste due to retarded hydration in the SRA system [32,33]) shows a single dominant freezing peak around −15 °C, the plain paste shows a significantly smaller peak at the same temperature and another peak which occurs around −43 °C. In the SRA paste, there is only evidence of a very small peak occurring around −47 °C in Fig. 5. The peak sizes at −15 °C suggest a much larger content of freezable water in the SRA system as compared to the plain system, potentially implying a greater extent of microstructural connectivity in the SRA system as compared to the plain system, in direct contrast to their similar chemical shrinkage results.

Other data indicates the persistence of the freezing peak around −15 °C in the SRA system up to 7 d, seemingly indicating that the porosity in these systems remains percolated [45,46]. This is obviously in contradiction to the chemical shrinkage measurements in Fig. 2 which indicate that by 24 h, both the plain and SRA systems have experienced a disconnection of their capillary porosity while porosity percolation is always maintained at some smaller (gel) pore-size scale. Taken together, the LTC results suggest that the presence of the SRA influences ice formation in the system and results in a potentially spurious interpretation of capillary porosity percolation-or-depercolation in cementitious systems containing SRA at early ages.

To further investigate the unique freezing (and melting) response of SRA pastes, experiments were performed on: (1) porous glasses having nominally mono-size pores (pore radius of 4 nm and 200 nm) to eliminate the stepped undercooling effects which manifest due to the wide distribution of pore sizes in cement pastes and (2) on solutions with and without SRA to understand the influence of the admixture on the freezing (and melting) behavior of bulk liquids. The glass pore sizes were selected so as to ensure that the SRA is able to infiltrate the pore system (e.g., calculations suggest that this SRA molecule has a radius of around 0.4 nm). Fig. 6(a) shows LTC freezing scans performed on the 200 nm glass saturated with DI-water and with a synthetic pore-solution with-or-without SRA. In each case, a single sharp freezing peak is observed that corresponds to the solution freezing in the mono-size pores in the material. The DI-water and the synthetic pore solution each show a freezing peak around −15 °C, implying that the composition of the pore solution has a minimal effect on the freezing behavior of the system [47]. In general, the addition of the SRA is seen to depress the freezing temperature with the depression being a function of the SRA concentration (i.e., freezing peaks around −18 °C and −27 °C for the 5% and 10% SRA solutions, respectively). A similar response is observed in the case of the 4 nm porous glass (Fig. 6(b)) wherein the freezing peaks corresponding to DI-water, 10%, and 20% SRA solutions appear around −22 °C, -36 °C, and −45 °C, respectively. The lower freezing temperatures observed in the case of the 4 nm glass is a function of its smaller pores. A similar response is noted in the case of melting as well (not shown), wherein the presence of the SRA is observed to progressively depress (to a more negative temperature) the melting point of the system.

Fig. 7(a) shows melting scans for bulk solutions of distilled water and 10% and 20% solutions by mass of the SRA. In the case of bulk solutions as well, the addition of the SRA is noted to progressively depress the melting (and freezing) temperature of the solution; with an increase in the SRA concentration. This may be as expected since a pure SRA solution does not freeze even upon cooling to −80 °C (not shown). The direct impact of the SRA on the freezing and melting point change can be analyzed by discriminating "bulk solution effects" from the melting response of solutions contained in the 4 nm porous glass as shown in Fig. 7(b). Here it is noted that, even when the "solution effect" (open squares) of the SRA is subtracted from the influence of the SRA on the melting point of a solution contained in
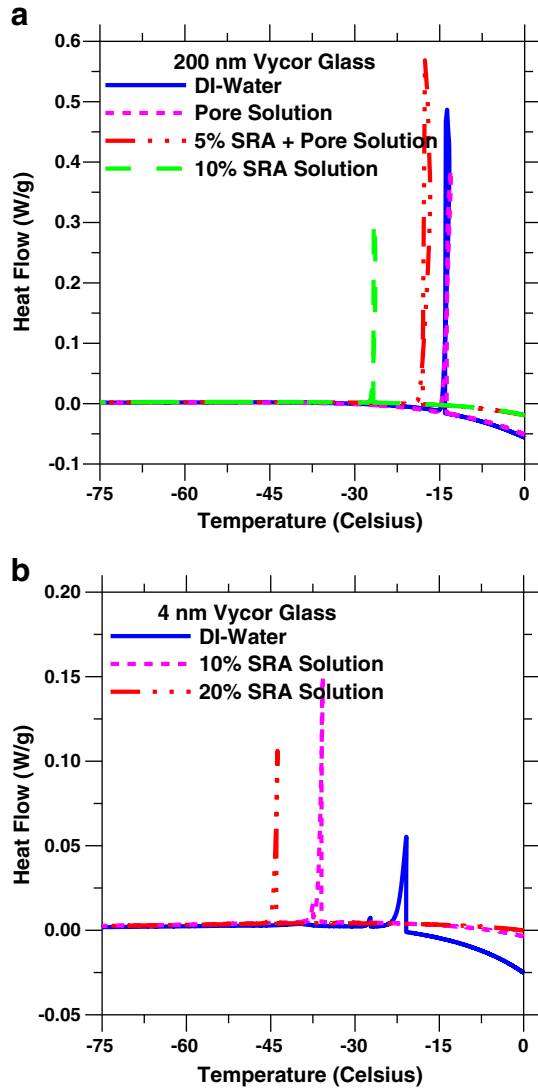

Fig. 5. Representative LTC scans for cement pastes illustrating the persistence of the −15 °C freezing peak in SRA containing pastes.

Fig. 6. LTC scans for porous glasses saturated with solutions with and without a SRA for: (a) 200 nm porous glass and (b) 4 nm porous glass.

Fig. 7. (a) Melting curves for solutions of de-ionized water and a solution containing SRA and (b) the influence of the SRA on the melting point change of bulk water and SRA solutions and solutions contained in the 4 nm porous glass.

the porous glass (open circles) the corrected response (solid squares) still sketches a linear-function with a finite (positive) slope.[5] This is an important point as if the melting (and freezing) response in the porous glass was singularly related to the properties of the solution the corrected response would sketch a curve which would lie approximately parallel to the abscissa axis indicating that the melting point depression is equivalent for bulk solutions and the solutions confined in the 4 nm porous glass. This response, wherein the shift in the melting temperature (Fig. 7(b)) for the bulk solutions is observed to be much smaller than that for melting of equivalent solutions in the 4 nm porous glass specimens suggests that, potentially, the solid–liquid surface-energy at the ice–liquid interface may be progressively modified (increased) with an elevation of the in solution SRA

concentration; while assuming that the changes in the adsorbed-film thickness are a second order contribution. It is this change in the surface energy that likely produces the alteration in the freezing (and melting) response in the 4 nm porous glass systems when the SRA is present.

In summary, the LTC scans performed on the porous glasses show a response that is contrary to the measurements performed on the cement pastes. This difference in behavior is attributed to the SRA acting as an anti-freeze agent in the porous glass where it depresses the freezing (and melting) temperature (likely by elevating the interfacial ice–water surface energy) and thus increasing the extent of supercooling [48,49]. However, in cement pastes, in spite of this elevation in the ice–water surface tension, the SRA appears to act as a nucleation agent for ice-formation and elevates the freezing temperature such that nearly all of the potentially freezable solution in the specimen is frozen near − 15 °C [50–52]. This ice-nucleation behavior in cement pastes has also been observed for another commercially available SRA, in addition to the one examined in the present study [45]. The freezing and melting response of porous glass and cement pastes with and without SRA is discussed in more detail in Section 5.3.

---

[5] Here it should be noted that, the temperatures identified in Fig. 7(b), for both solutions and glasses correspond to the temperature associated with the absolute maximum (peak) heat flow value. While it may be argued that this is not a unique point related to the initiation or completion of the phase transformation (melting), for the sake of consistency the authors have chosen to use this temperature as it is numerically well-defined.
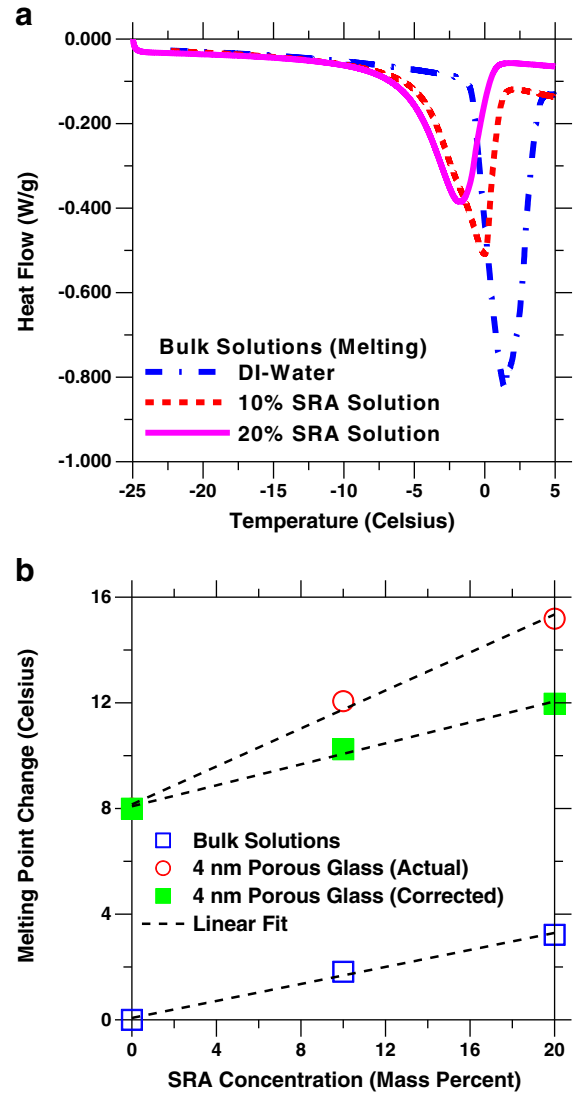
a

Thin Specimen
(Initial)

Saturated Depth

Thin Specimen
(Final)

Saturated Depth

Thick Specimen
(Initial)

Saturated Depth

Thick Specimen
(Final)

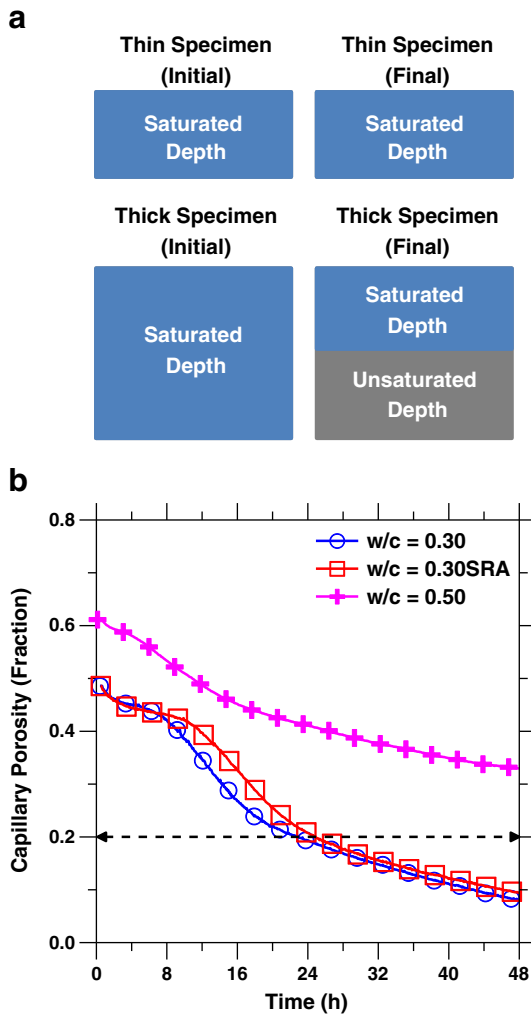| Saturated
Depth |
|---|
| Unsaturated
Depth |

b

Fig. 8. (a) An illustration of the change in the degree of fluid saturation as a function of depth and hydration in thin and thick specimens and (b) The capillary porosity as a function of time. The dashed line indicates the depercolation threshold proposed by Powers and co-workers [15,16].

5. Discussion of experimental results

5.1. Size dependence in chemical shrinkage measurements

The thickness dependent deviation in chemical shrinkage (Fig. 2) can be explained by considering the cases of a thin and a thick specimen which are absorbing water (Fig. 8(a)). Initially, the paste is fresh (plastic) and fluid-saturated. As hydration progresses and vapor filled spaces grow and coalesce in the material (around set), water ponded at the surface is able to permeate through the paste and maintain saturation in both thin and thick sections [34,53]. With increasing hydration, the thin section is able to have water permeate through its thickness, maintaining saturation and thereby demonstrating a continuous increase in chemical shrinkage. However, with increasing hydration in the thick section, a combination of effects due to a global porosity decrease and a decrease in connectivity of the capillary pores due to hydration impedes the movement of water resulting in a plateau in chemical shrinkage. In these thicker low w/c specimens, this will produce self-desiccation and may amplify the risk of early-age cracking.

Fig. 8(b) shows the evolution of the capillary porosity with time for the systems evaluated in Fig. 2, computed using their degree of hydration and Jensen's formulation of Powers model, assuming that the capillary porosity is equivalent to the volume of capillary water

contained in the material [24,54]. In general, a non-linear decrease in the capillary porosity is observed with increasing time, while a linear decrease is observed with increasing hydration. The non-linear response can be used to relate the time interval of the chemical shrinkage deviation (Fig. 2) to the residual porosity at a given time (degree of hydration). The results suggest that the plain and SRA pastes depercolate at about 18 h and 21 h, respectively, corresponding to a residual capillary porosity of approximately 23% (36% hydration) in each case, while the w/c = 0.50 paste is expected to retain a percolated structure during the first 48 h of hydration. These results quantitatively confirm the validity of the porosity-based depercolation criterion suggested by Powers and co-workers [15]. However, rather than a fixed porosity value of 20%, it is more meaningful to consider a depercolation criterion in the residual porosity range between 15% and 25% [55]. It should be noted that the porosity-based depercolation criteria is most clearly linked to a reduction in the fluid-permeability of the material, as per Powers' original experiments. This is significant in that, these results are in stark contrast to the results of other fluid-permeability experiments performed on previously dried specimens and computer-based numerical simulation studies published in the literature that suggest that the capillary porosity in cement pastes does not depercolate until around 3% to 5% residual porosity [17,56]. This is especially significant as the damage induced during drying of cementitious specimens has been previously demonstrated to repercolate the capillary pore networks [18,57].

5.2. The interpretation of electrical conductivity measurements to identify capillary porosity depercolation in cementitious materials

The electrical conductivity of cement paste, mortar and concrete has been extensively modeled using the modified parallel law [29]. This relationship is described in Eq. (2) and will be used to interpret the electrical conductivity measurements shown in Fig. 3.

$$\sigma_t = \sigma_0 \phi \beta \qquad (2)$$

where: σ_t is the bulk cement paste conductivity (S/m), σ_o is the pore solution conductivity (S/m), ϕ is the volume fraction of the fluid contained in the pores (gel and capillary), and β is a factor that describes the pore fluid connectivity. Fig. 9(a) shows the bulk paste conductivity as a function of the capillary porosity in the cement pastes. For all mixtures, the bulk conductivity decreases rapidly with a decrease in the capillary porosity due to increasing hydration. It is interesting to note that, while the low w/c mixtures quickly approach the depercolation threshold (15%–25% porosity), the w/c = 0.50 mixture is not able to reach this level of capillary porosity during the time period of the experiments, due to its larger initial capillary porosity. The w/c = 0.30 and w/c = 0.30SRA mixtures show conductivities around 0.14 S/m and 0.12 S/m, respectively, at the point of the chemical shrinkage deviation (23% porosity). This suggests that an electrical conductivity lower than 0.15 S/m may indicate a disconnected pore system in ordinary portland cement pastes of intermediate alkali content as used in this study. On the other hand, the w/c = 0.50 paste shows a conductivity value higher than 0.20 S/m, even when cured under saturated conditions for 18 months [58].

The measured conductivities of the paste and pore solution can be used to compute the formation factor, which can be related to the transport properties of a porous medium such as fluid-permeability and ion-diffusion coefficients [29,59]. The formation factor (F) when plotted as a function of the capillary porosity describes the connectivity of the pores independent of changes in the fluid conductivity; where a higher value indicates a less connected pore system.

$$F = \frac{\sigma_0}{\sigma_t} \qquad 3(a)$$
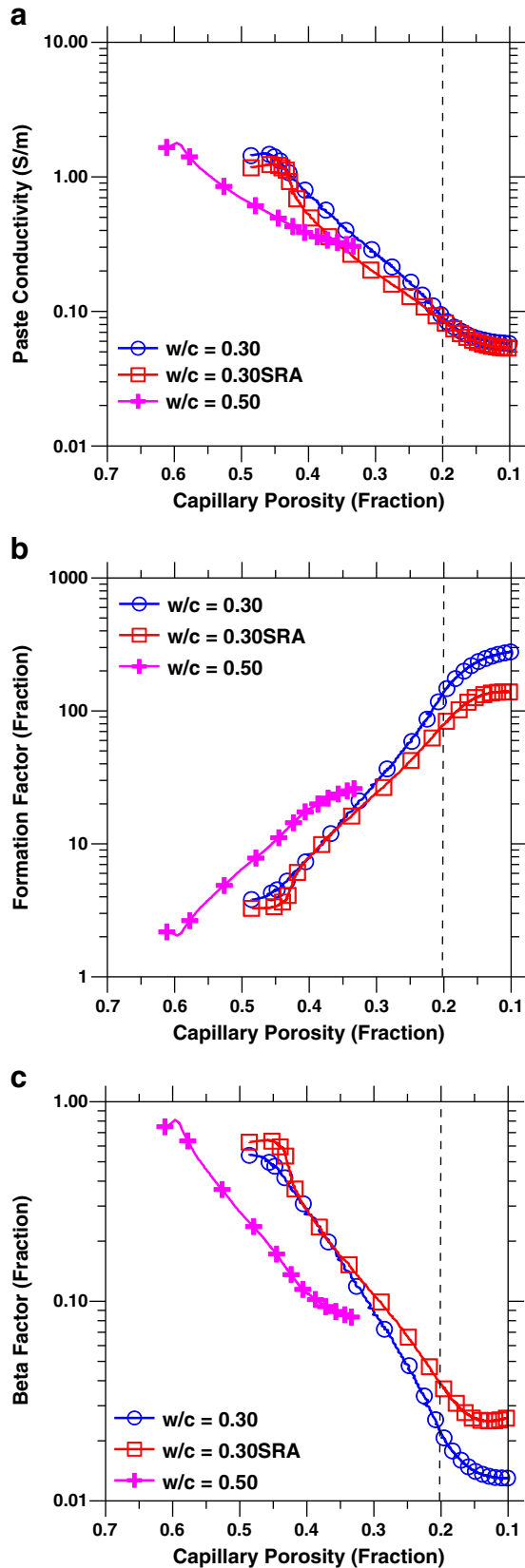
Fig. 9. (a) The electrical conductivity as a function of the capillary porosity, (b) The formation factor as a function of the capillary porosity and (c) The Beta factor (moisture connectivity) as a function of the capillary porosity. The dashed line on the graphs indicates the capillary porosity-based depercolation threshold proposed by Powers and co-workers [15,16].

where: F is a parameter known as the formation factor (fraction), a function of the porosity and the configuration of the fluid-filled pore structure for materials which display insignificant surface conduction [29]. The configuration of the pores includes descriptions of the constrictivity and the tortuosity of the pore system. Fig. 9(b) shows the evolution of the formation factor for the three cement pastes. The formation factor increases almost linearly with a decrease in the capillary porosity and at an equivalent degree of hydration (i.e., 30%) scales as 0.30(37.44)>0.30SRA(29.29)>0.50(9.72) suggesting that the connectivity of the pores and the fluid-permeability of the materials scales in the inverse order [29,59]. This point is validated by mercury intrusion porosimetry (MIP) analysis of the cement pastes which indicates that, while the w/c = 0.50 mixture has the least dense pore system, the w/c = 0.30 and w/c = 0.30SRA mixtures show essentially equivalent pore systems (pore volume and critical diameter) [60]. This agrees with theory where F decreases toward unity with increasing and more connected porosity. A clearer assessment of the connectivity of moisture in the microstructure emerges when the pore fluid connectivity (β) described in Eq. (3b) is plotted versus the capillary porosity:

$$\beta = \frac{\sigma_t}{\sigma_0 \phi}. \qquad \text{3b}$$

Here the volume fraction (ϕ) of the pore solution is computed using the measured degree of hydration and Jensen's formulation of Powers model, while the other parameters are measured directly [24,54]. The change in the connectivity of the pore-fluid (β) as a function of the capillary porosity is described in Fig. 9(c). In general, the pore fluid connectivity decreases with increasing hydration (decreasing porosity) until an almost constant value is achieved. It is important to note that the connectivity factor at 48 h for the low *w/c* mixtures is approximately one order of magnitude lower than that for the high *w/c* mixture. These results suggest that the distribution and connectivity of the capillary porosity in these materials is considerably different.

5.3. The influence of SRAs on interpreting capillary depercolation in cement pastes using LTC

As discussed previously, the freezing response observed during LTC measurements of SRA containing cement pastes could produce a different interpretation of capillary depercolation than that indicated by the chemical shrinkage measurements. For example, for a plain cement paste (*w/c* = 0.30), the freezing peak height (i.e., peak–baseline) at −15 °C extracted from the LTC scans shows a progressive reduction in magnitude (equivalent to the volume of connected freezable water) with increasing maturity; reducing almost to zero around 24 h [61]. In contrast, the freezing peak height in the SRA system does not approach zero until almost 5 d to 7 d (for a SRA dosage around 5% by replacement of the initial mixing water; see Fig. 5 and [45]). As such, while LTC measurements of the plain system qualitatively indicate depercolation to occur around 24 h, similar to the chemical shrinkage measurements, LTC scans of the SRA system appear to indicate the persistence of a percolated pore system in direct contradiction to the chemical shrinkage response of the SRA paste. The behavior of the SRA in hydrated cement paste is also in contrast to its behavior in the porous glass specimens, where the freezing peak temperature is consistently lowered. Two possibilities will be considered to explain these results, namely: (1) a modification of the pore sizes and their connectivity (the pore-structure) due to the presence of the SRA and-or (2) the potential of the SRA to act as an ice-nucleation agent.

In the first case, it would be required that the LTC and the chemical shrinkage results are controlled by two different sizes of pores in order to explain the similarity of the SRA/non-SRA chemical shrinkage
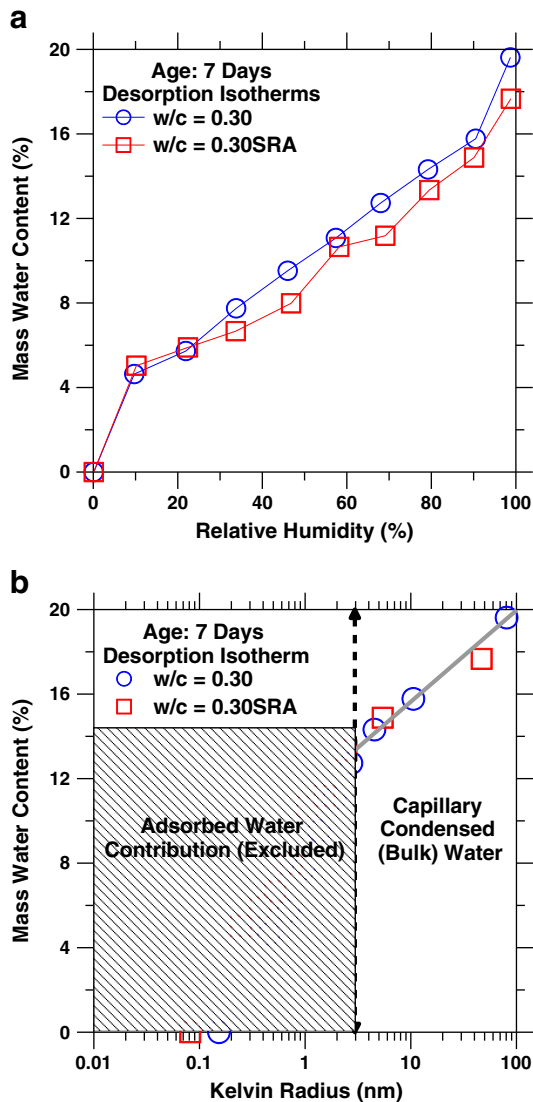
Fig. 10. (a) The first desorption isotherm for plain and 5% SRA containing cement pastes and (b) The governing Kelvin radius as a function of the desorbed water content, wherein, the Kelvin radius is determined after considering the influence (reduction) of the SRA on the surface tension at the liquid–vapor interface. [6] The dashed line shows the dimensional thermodynamic stability limit of the interfacial liquid–vapor meniscus at a Kelvin Radius of around 3 nm [8,62–64].

results in light of their differences in LTC. Mercury intrusion porosimetry has previously indicated that SRA and non-SRA pastes have essentially similar pore structures [60]. This point is confirmed by first desorption isotherms (Fig. 10(a)) measured on saturated cement paste specimens[7] (T = 25 °C) with no prior drying determined using a dynamic water vapor sorption (DVS-1) analyzer for plain and SRA pastes from 98 to 0% RH in 10% RH steps using a stability criterion of 0.001%/min (where % denotes the ratio of the instantaneous measured mass to the dry sample mass as a percentage) or alternately a maximum equilibration time of 960 min (16 h) at each RH step. It should be noted that the cement paste samples prepared for

---

[6] It should be noted the RH inversion to the Kelvin radius through the Kelvin–Laplace relation considers that at the present dosage level (5% SRA), the addition of the SRA reduces the interfacial liquid–vapor surface tension by approximately a factor of 2 [8,58]. The remaining parameters in the Kelvin–Laplace relation remain unchanged.

[7] It should be noted that the 7 day old cement paste samples were powdered and sieved through a 100 micrometer sieve prior to determination of the desorption spectrum. Typically an initial powder mass in the range of 30– 60 mg was used in the analysis.

determination of the desorption isotherm did not contain any HRWRA and were cured under saturated conditions at 20 °C in lime water (plain paste) or lime water and 5% SRA solutions (SRA paste), to maintain saturated curing conditions and minimize (SRA) leaching concerns, for 7 days prior to measurement of their desorption spectrums.

When the first desorption isotherm is corrected[8] for the influence of the SRA on the interfacial liquid–vapor surface tension of the pore solution and inverted to reveal the size of pores (or more correctly the Kelvin radius at a specific relative humidity level) containing capillary-condensed water (i.e., RH>70% and RH>85% for the plain and SRA systems respectively, Fig. 10(b) [8,65–67]) it is determined that, broadly, pastes with and without SRA display essentially similar pore systems at the size scale of interest, namely a Kelvin radius ranging between 5 nm and 50 nm.[9] Consequently, differences in the capillary pore structure caused by the SRA are likely not the reason for the observed differences of the LTC and chemical shrinkage responses[10] [8,61,68].

The second explanation of enhanced nucleation of ice due to the presence of the SRA would require consideration of why this nucleation does not occur in the porous glass systems as well. Polymer adsorption isotherms and zeta potential measurements performed on cement particles-and-hydrates in surfactant-water solutions indicate that non-ionic surfactants do not adsorb significantly on cement particles-and-hydrates, but do adsorb in considerable quantities on silica surfaces [69–71]. It should be noted that, the surfactant used in [69], TX405, Dow Chemical, to measure adsorption isotherms, is similar in type and molecular weight to the SRA used in this study [72]. In cement systems, there is evidence to suggest that SRAs of certain chemistries are incorporated into the structure of the hydration products as illustrated by the thermogravimetric analysis (TGA) curves provided in Fig. 11 [30]. For the cement paste with SRA, the SRA is released at a much higher temperature (around 300 °C and between 600 °C to 800 °C) than that necessary for evaporating it from a bulk solution (200 °C). This strong interaction between hydration products and organic molecules has also been noted in the case of polyethylene glycols by Beaudoin et al. [73]. This leads to the hypothesis that SRA molecules that exist in the pore solution or the hydration products may arrange in and-or along the pore-walls in cement pastes containing SRAs, such that these molecules are "suitably-oriented" to serve as ice nucleation agents. In this way, water within the capillary pores that would normally freeze at a lower (negative) temperature due to being surrounded by smaller pore entryways (ink-bottle effects) freezes at elevated (less negative) temperatures around −15 °C.

However, at later ages, as the SRA (in solution) is progressively consumed due to incorporation in the hydration products, new hydration products will form that contain few (if any) SRA molecules within their structure. These hydration products (and the pore solution) are thus similar to those in the non-SRA pastes and will exhibit a similar freezing behavior with freezing peaks at lower (more negative) temperatures. This is consistent with the appearance of the

---

[8] It should be noted, in addition to the surface tension reduction effects of the SRA, the presence of dissolved species (ions) also produces a much smaller (second order) reduction in the surface tension of the pore solution [8].

[9] Strictly speaking, determination of pore sizes (and their distributions) using vapor sorption isotherms requires a description of both the Kelvin radius and the thickness of the adsorbed water layer (i.e., the t-curve [66,67]). However, since in the capillary-condensation regime the Kelvin radius is far larger than the adsorbed water thickness, at a first approximation, the t-curve contribution to the pore-size description is assumed equivalent in the case of plain and SRA containing systems.

[10] It should be noted that these interpretations do not consider the potential adsorption-or-uptake of the SRA in the capillary condensation regime (RH>70%), when considerable free water (and mobile SRA) is present. However, even if adsorption-or-uptake were to be considered (by assuming a systematic change of the SRA content and thus surface tension of the pore solution; up to a limiting value) this does not considerably alter the interpretation of the desorption response and-or the Kelvin radius description in the capillary condensation regime.

a

b
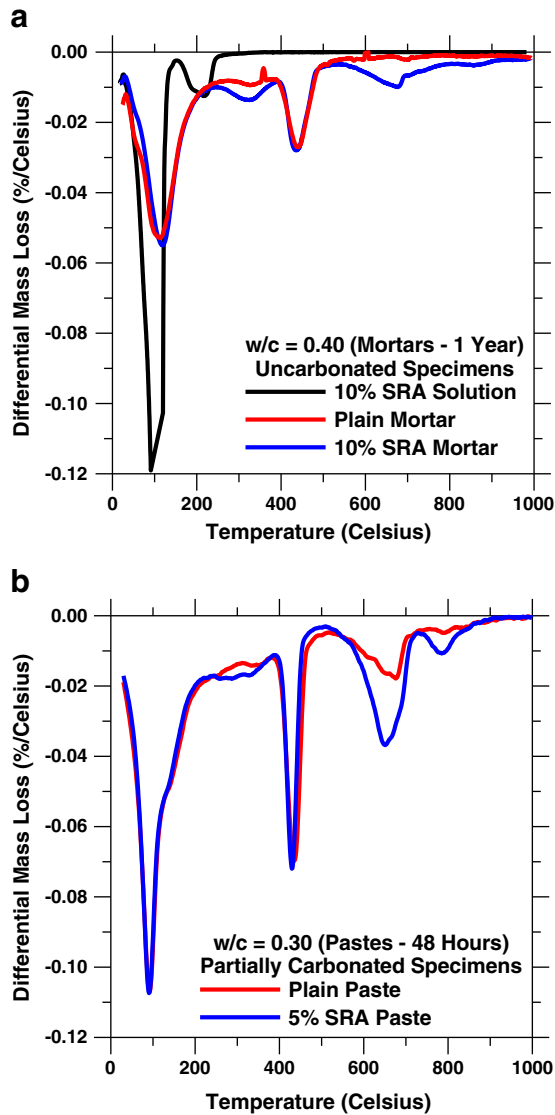
Fig. 11. Thermogravimetric analysis of: (a) uncarbonated cement mortars with and without SRA, along with that of a bulk SRA solution. The mass values for the solution have been divided by a factor of 10 to appear on the same scale as the mortar datasets and (b) partially carbonated cement pastes with and without SRA [33,61].

lower temperature peaks at later ages in cement pastes containing SRA [42]. It has further been noted that the higher the initial SRA dosage, the longer the time before which these 2nd and 3rd peaks appear [42]. Thus, this argument provides a potentially self-consistent explanation for the observed LTC behavior of the systems with SRA by combining aspects related to surfactant adsorption and-or mobility and microstructural geometry to completely describe the freezing response of pastes containing SRAs. In summary, in the case of early-age cement pastes, the nucleation agent response of the SRA eliminates the influence of ink bottle pores on the LTC response, and thus negates the use of LTC to detect capillary porosity depercolation in cementitious materials containing SRAs.

6. Summary and conclusions

This investigation has utilized several techniques to identify capillary porosity depercolation in cement-based materials.

- Measurements of chemical shrinkage performed on cement pastes indicate the age at which the experimental response demonstrates a

thickness (size) dependent deviation. This deviation occurs when the capillary porosity is reduced to around 15%–25%. These observations validate the depercolation criterion first proposed by Powers and co-workers [15] based on measurements of fluid-permeability, which suggests that the depercolation of the pore-structure occurs around 20% capillary porosity in cement pastes. This contradicts other results in the literature [17,51] that indicate capillary depercolation at 3% to 5% capillary porosity in cement pastes (which are dried prior to permeability evaluations).

- Electrical measurements indicate that a measured electrical conductivity lower than 0.15 S/m at approximately 20% capillary porosity is consistent with a depercolated pore system in the ordinary portland cement pastes examined in this study. This disconnection of the capillary pore system is strongly related to the reduction in transport, as originally inferred by Powers and co-workers [15,16,74] with their fluid-permeability measurements.

- A critical analysis of LTC measurements suggests that this technique, while valid to assess depercolation in neat cement pastes, is not applicable for more complex systems containing organic admixtures (i.e., SRAs) which may induce ice nucleation action. Despite this limitation, LTC can be used for determining the cumulative freezable water content in cementitious systems with and without chemical admixtures.

References

[1] A. Bentur, Early age cracking in cementitious systems, in: A. Bentur (Ed.), RILEM State of the Art Report TC-EAS, 2002.
[2] P.D. Krauss, E.A. Rogalla, M.R. Sherman, D.B. McDonald, A.E.N. Osborn, D.W. Pfeifer, NCHRP Report 380, Transverse Cracking in Newly Constructed Decks. NCHRP Project, 1995, pp. 12–37.
[3] O.M. Jensen, P. Lura, Techniques and materials for internal water curing of concrete, Materials and Structures 39 (9) (2006) 817–825.
[4] D.P. Bentz, P. Lura, J. Roberts, Mixture proportioning for internal curing, Concrete International 27 (2) (2005) 35–40.
[5] A. Radlinska, F. Rajabipour, B. Bucher, R. Henkensiefken, G. Sant, W.J. Weiss, Shrinkage mitigation strategies in cementitious systems: a closer look at sealed and unsealed behavior, The Transportation Research Record 2070 (2008) 59–67.
[6] http://www.dot.ca.gov/hq/esc/Translab/pubs/CPC2001/JeffAbercrombie.pdf, June 30 2009.
[7] http://www.fhwa.dot.gov/construction/reviews/revdeck2.cfm, June 30 2009 last verified.
[8] W.J. Weiss, P. Lura, F. Rajabipour, G. Sant, Performance of shrinkage reducing admixtures at different humidities and at early ages, ACI Materials Journal 105 (5) (2008) 478–486 September-October.
[9] S.P. Shah, W.J. Weiss, W. Yang, Shrinkage cracking — can it be prevented? Concrete International 20 (4) (1998) 51–55.
[10] D. Bentz, M. Geiker, K. Hansen, Shrinkage-reducing admixtures and early-age desiccation in cement pastes and mortars, Cement and Concrete Research 31 (7) (2001) 1075–1085.
[11] The Klein Symposium on expansive cements, ACI Special Publication (SP-38), The American Concrete Institute, Detroit, Michigan, USA, 1973.
[12] J. Olek, M.D. Cohen, Procedure for mixture proportioning of type-k expansive cement blends for use in shrinkage-compensating mortars, ACI Mat Journal (1991) 536–543 September-October.
[13] P. Lura, D.P. Bentz, D. Lange, K. Kovler, A. Bentur, K. van Breugel, Measurement of water transport from saturated pumice aggregates to hardening cement paste, Materials and Structures 39 (9) (2006) 861.

[14] R. Henkensiefken, T. Nantung, W.J. Weiss, 'Saturated Lightweight Aggregate for Internal Curing in Low w/c Mixtures: Monitoring Water Movement Using X-ray Absorption', Strain, 47 (2009) 1–10, doi:10.1111/j.1475-Q137481305.2009.00626.x.

[15] T.C. Powers, L.E. Copeland, H.M. Mann, Capillary continuity or discontinuity in cement pastes, The Research Bulletin of the Portland Cement Association 1 (2) (1959) 38–48 Bulletin 110.

[16] T.C. Powers, L.E. Copeland, J.C. Hayes, H.M. Mann, 'Permeability of portland cement paste', Bulletin 53, Journal of the American Concrete Institute 51 (1955) 285–298.

[17] G. Ye, Percolation of capillary pores in hardening cement pastes, Cement and Concrete Research 35 (2005) 167–176.

[18] H.F.W. Taylor, Cement Chemistry, 2nd Edition Thomas Telford, United Kingdom, 1997.

[19] D.P. Bentz, Capillary porosity depercolation/repercolation in hydrating cement pastes via low-temperature calorimetry measurements and CEMHYD3D modeling, Journal of the American Ceramic Society 89 (8) (2006) 2606–2611.

[20] Geiker, M., 'Studies of Portland Cement Hydration: Measurement of Chemical Shrinkage and a Systematic Evaluation of Hydration Curves by Means of the Dispersion Model', PhD Thesis, Technical University of Denmark, Lyngby, Denmark, (1983).

[21] G. Sant, P. Lura, W.J. Weiss, Measurement of volume change in cementitious materials at early ages: review of testing protocols and interpretation of results, The Transportation Research Record 1979 (2006) 21–29.

[22] G. Sant, C.F. Ferraris, W.J. Weiss, Rheological property measurements of cement pastes at early ages: a discussion of structure formation and mechanical property development, Cement and Concrete Research 38 (11) (2008) 1286–1296.

[23] R.A. Helmuth, L.M. Hills, D.A. Whiting, S. Bhattacharja, Abnormal Concrete Performance in the Presence of Admixtures', PCA Serial # 2006, 1995.

[24] O.M. Jensen, P.F. Hansen, Water-entrained cement-based materials; I. Principles and theoretical background, Cement and Concrete Research 31 (4) (2001) 647–654.

[25] G. Sant, F. Rajabipour, P. Fishman, P. Lura, W.J. Weiss, Electrical conductivity measurements in cement paste at early ages: a discussion of the contribution of pore solution conductivity, volume, and connectivity to the overall electrical response, International RILEM workshop on Advanced Testing of Fresh Cementitious Materials, 2006, pp. 213–222, Stuttgart, Germany.

[26] F. Rajabipour, W.J. Weiss, D. Abraham, Insitu electrical conductivity measurements to assess moisture and ionic transport in concrete, Advances in Concrete through Science and Engineering, International RILEM Symposium, Evanston, Illinois, 2004, p. 10.

[27] Penko, M., 'Some Early Hydration Processes in Cement Pastes as Monitored by Liquid Phase Composition Measurements', PhD Dissertation, Purdue University, West Lafayette, Indiana, USA, (1983).

[28] R.S. Barneyback Jr., S. Diamond, Expression and analysis of pore fluids from hardened cement paste, Cement and Concrete Research 11 (2) (1981) 279–285.

[29] B.J. Christensen, R.T. Coverdale, R.A. Olson, S.J. Ford, E.J. Garboczi, H.M. Jennings, T.O. Mason, Impedance spectroscopy of hydrating cement-based materials: measurement, interpretation, and application, Journal of the American Ceramic Society 77 (11) (1994) 2789–2802.

[30] P. Acker, V. Baroghel-Bouny, S. Garcia, Can water be the glue?, 2nd international RILEM workshop: why does cement set? in: A. Nonat (Ed.), An Interdisciplinary Approach, 2000, pp. 23–36.

[31] D.P. Bentz, Three-dimensional computer simulation of portland cement hydration and microstructure development, Journal of the American Ceramic Society 80 (1) (1997) 3–21.

[32] F. Rajabipour, G. Sant, W.J. Weiss, Interactions between shrinkage reducing admixtures and cement paste's pore solution, Cement and Concrete Research 38 (5) (2008) 606–615.

[33] G. Sant, B. Lothenbach, P. Juilland, G. LeSaout, K. Scrivener, W.J. Weiss, The origin of early-age expansions induced in cement pastes containing shrinkage reducing admixtures, Cement and Concrete Research 41 (2011) 218–229.

[34] G. Sant, M. Dehadrai, D. Bentz, P. Lura, C.F. Ferraris, J. Bullard, W.J. Weiss, Detecting the fluid-to-solid transition in cement pastes, Concrete International (June 2009) 43–48.

[35] P. Mounanga, V. Baroghel-Bouny, A. Loukili, A. Khelidj, Autogenous deformations of cement pastes: part 1. Temperature effects at early age and micro–macro correlations, Cement and Concrete Research 36 (1) (2006) 110–122.

[36] V. Baroghel-Bouny, P. Mounanga, A. Khelidj, A. Loukili, N. Rafai, Autogenous deformations of cement pastes: part 2. W/C effects, micro–macro correlations and threshold values, Cement and Concrete Research 36 (1) (2006) 123–136.

[37] Fu, T., 'Autogenous Deformation and Chemical Shrinkage of High Performance Cementitious Systems', Master's Thesis, Oregon State University, Corvallis, Oregon, pp. 147, (2011).

[38] B. Johannesson, Dimensional and ice content changes of hardened concrete at different freezing and thawing temperatures, Cement and Concrete Composites 32 (1) (2010) 73–83.

[39] K.A. Snyder, D.P. Bentz, Suspended hydration and loss of freezable water in cement pastes exposed to 90% relative humidity, Cement and Concrete Research 34 (2004) 2045–2056.

[40] Z. Sun, G.W. Scherer, Pore size and shape in mortar by thermoporometry, Cement and Concrete Research 12 (2010) 740–751.

[41] G.W. Scherer, Freezing gels, Journal of Non-Crystalline Solids 155 (1993) 1–25.

[42] M. Brun, A. Lallemand, J.F. Quinson, C. Eyraud, A new method for the simultaneous determination of the size and shape of pores: the thermoporometry, Thermochimica Acta 21 (1977) 59–88.

[43] G. Fagerlund, Determination of pore-size distribution from freezing-point depression, Materials and Construction 6 (33) (1973) 215–225.

[44] Villadsen, J., 'Pore Structure in Cement-Based Materials', PhD Thesis, Technical University of Denmark, Lyngby, Denmark, (1992).

[45] D.P. Bentz, Influence of shrinkage-reducing admixtures on early-age properties of cement pastes, Journal of Advanced Concrete Technology 4 (3) (2006) 423–429.

[46] D.P. Bentz, P.E. Stutzman, Curing, hydration, and microstructure of cement pastes, ACI Materials Journal 103 (5) (2006) 348–356.

[47] J.P. Acker, J.A.W. Elliot, L.E. McGann, Intercellular ice propagation: experimental evidence for ice growth through membrane pores, Biophysical Journal 81 (2001) 1389–1397.

[48] B. Zobrist, U. Weers, T. Koop, Ice nucleation in aqueous solutions of poly-ethylene glycol with different molar mass, Journal of Chem. Physics 118 (22) (2003) 10254–10261.

[49] B. Zobrist, C. Marcolli, T. Peter, T. Koop, Heterogeneous ice nucleation in aqueous solutions: the role of water activity, Journal of Phys. Chem. A 112 (2008) 3965–3975.

[50] M. Gavish, Biro Popovitz, M. Lahav, L. Leiserowitz, Ice nucleation by alcohols arranged in monolayers at the surface of water drops, Science, New Series 250 (4983) (November 16 1990) 973–975.

[51] N. Fukuta, B.J. Mason, Epitaxial growth of ice on organic crystals, Journal of the Physics and Chemistry of Solids 24 (1963) 715–718 Pergamon Press.

[52] B. Zobrist, T. Koop, B.P. Luo, C. Marcolli, T. Peter, Heterogeneous ice nucleation rate coefficient of water droplets coated with a nonadecanol layer, Journal of Physical Chemistry C 111 (2007) 2149–2155.

[53] P. Lura, J. Couch, O.M. Jensen, W.J. Weiss, Early-age acoustic emission measurements in hydrating cement paste: evidence for cavitation during solidification due to self-desiccation, Cement and Concrete Research 39 (10) (2009) 861–867.

[54] T.C. Powers, T.L. Brownyard, 'Studies of the Physical Properties of Hardened Portland Cement Paste', Bulletin 22, Research and Development Laboratories of the Portland Cement Association, Chicago, Illinois, 1948.

[55] E.J. Garboczi, D.P. Bentz, Computer simulation of the diffusivity of cement-based materials, Journal of Materials Science 27 (1992) 2083–2092.

[56] G. Ye, K. Van Breugel, A.L.A. Fraaij, Three-dimensional microstructure analysis of numerically simulated cementitious materials, Cement and Concrete Research 33 (2003) 215–222.

[57] D.H. Bager, E.J. Sellevold, Ice formation in hardened cement paste, Part II— drying and resaturation of room temperature cured pastes, Cement and Concrete Research 16 (1986) 834–844.

[58] Rajabipour, F., 'Fundamental Investigations on Utilizing Electrical Sensing to Improve Life Cycle Modeling of Concrete Structures', MSCE Thesis, Purdue University, pp. 105, (2003).

[59] A.J. Katz, A.H. Thompson, Quantitative prediction of permeability in porous rock, Physical Review 34 (11) (1986) 8179–8181.

[60] G. Sant, J. Lovell, J. Weiss, Mercury Intrusion Porosimetry of Ordinary Portland Cement Pastes: Unpublished Results, Purdue University, West Lafayette, IN, 2006–2009.

[61] Sant, G., 'Fundamental Investigations Related to the Mitigation of Volume Changes in Cementitious Materials at Early Ages', PhD Dissertation, Purdue University, West Lafayette, IN, USA, pp. 226, (2009).

[62] E.P. Barrett, L.G. Joyner, P.P. Halenda, The determination of pore volume and area distributions in porous substances I: computations from nitrogen isotherms, Journal of the American Chemical Society 73 (1951) 373–380.

[63] J. Hagymassy, S. Brunauer, R.S.H. Mikhail, Pore structure analysis by water vapor adsorption I: t-curves for water vapor, Journal of Colloid and Interface Science 29 (3) (March 1969) 485–491.

[64] R. Badmann, N. Stockhausen, M.J. Setzer, The statistical thickness and the chemical potential of adsorbed water films, Journal of Colloid and Interface Science 82 (2) (August 1981) 534–542.

[65] G. Sant, A. Eberhardt, D. Bentz, W.J. Weiss, The influence of shrinkage reducing admixtures (SRAs) on moisture movement in cementitious materials at early ages, The ASCE Journal of Materials in Civil Engineering 22 (3) (March 2010) 10.

[66] F. Merlin, H. Guitouni, H. Mouhoubi, S. Mariot, F. Vallee, H. Van Damme, Adsorption and heterocoagulation of nonionic surfactants and latex particles on cement hydrates, Journal of Colloid and Interface Science 281 (2005) 1–10.

[67] P. Levitz, H. Van Damme, D. Keravis, Fluorescence decay study of the adsorption of nonionic surfactants at the solid– liquid interface 1: structure of the adsorption layer on a hydrophilic solid, The Journal of Physical Chemistry 88 (1986) 2228–2235.

[68] P. Levitz, H. Van Damme, D. Keravis, Fluorescence decay study of the adsorption of nonionic surfactants at the solid–liquid Interface 1: influence of polar chain length, The Journal of Physical Chemistry 90 (1986) 1302–1310.

[69] BASF Construction Chemicals: Tetraguard AS20 (Shrinkage Reducing Admixture): MSDS, http://www.basfadmixtures.com/SiteCollectionDocuments/MSDS/Specialty/Tetraguard%20AS20_MSDS.pdf: July 8, 2009 last verified.

[70] J.J. Beaudoin, H. Drame, L. Raki, R. Alizadeh, Formation and properties of C-S-H-PEG nanostructures, Materials and Structures 42 (2009) 1003–1014.

[71] T.C. Powers, T.L. Brownyard, Studies of the physical properties of hardened portland cement paste, Journal of the American Concrete Institute 18 (7) (March 1947) 845–880.

[72] L. Fischer, J. Israelachivili, Experimental studies on the applicability of the Kelvin equation to highly curved concave menisci, Journal of Colloid and Interface Science 80 (2) (1981).

[73] L. Fischer, J. Israelachivili, Direct measurement of the effect of meniscus forces on adhesion: a study of the applicability of macroscopic thermodynamics to microscopic liquid interfaces, Journal of Colloids and Surfaces 3 (1981) 303–319.

[74] R. Digilov, The Kelvin equation for meniscuses of nanosize dimensions, Langmuir 16 (2000) 1424–1427.